

Lyman Alpha Absorption Lines from Mini Pancakes

Biman B. Nath

Inter-University Centre for Astronomy & Astrophysics, Post Bag 4, Pune 411007, India

ABSTRACT

Recent numerical simulations show that many Ly α absorption lines of column densities $N_{\text{HI}} \lesssim 10^{15} \text{ cm}^{-2}$ are produced in transient, mini pancakes. Such pancakes are modeled here, approximating the initial perturbation leading to the formation of the pancake as a single sinusoidal wave. The density and temperature profiles of the gas in the pancake are determined in the case where cooling and heating rate of the gas is larger than the Hubble time, which is shown to hold for $z_c \sim 3$, where z_c is the collapse redshift. The Ly α absorption line profiles for a line of sight through the pancake are then calculated. The absorption lines in general have wings signifying bulk motions in the gas. It is shown that the deviation from a single Voigt profile is large for small H I column density lines, in which the effect of bulk motions is large. For lines with $N_{\text{HI}} > 10^{13} \text{ cm}^{-2}$, high temperature tend to wash out the signatures of bulk motion.

The analytical modeling of mini pancakes associated with Ly α forest lines— with $10^{13} \lesssim N_{\text{HI}} \lesssim 10^{15} \text{ cm}^{-2}$ —gives the corresponding mass scales. In structure formation models with CDM and with reheated IGM, the gas in the IGM is inhibited from falling into dark matter potential wells with very small velocity dispersions. Structures with masses larger than this limit (the Jeans mass) can have infall of gas and form

mini pancakes. It is shown here that, for typical values of cosmological parameters, absorption lines with $N_{\text{HI}} \sim 10^{14} \text{ cm}^{-2}$ correspond to structures with baryonic mass of $M_b \sim 10^{10} M_{\odot}$ with an overdensity of ~ 10 at $z \sim 3$. The value of N_{HI} can change by a factor ~ 3 in the course of evolution of the pancake in time. It is also shown that there is an upper limit to N_{HI} from a pancake due to the slow recombination rate and the importance of collisional ionization at high temperatures. Mini pancakes do not give rise to Ly α lines with $N_{\text{HI}} \gtrsim 10^{14.5} \text{ cm}^{-2}$, for a temperature of the IGM of $\bar{T} = 10^4 \text{ K}$, $J_{-21} = 1$ and $\Omega_{IGM} \sim 0.03$.

Subject headings: intergalactic medium - quasars : absorption lines - cosmology : miscellaneous

1. INTRODUCTION

Several ideas for the physical condition of the regions producing QSO absorption lines with low H I column density (the Ly α forest lines) have been proposed in the past. They have been, to name a few, pressure confined gas (Sargent et al.1980; Ostriker and Ikeuchi 1983), gas behind intergalactic shock waves (Vishniac and Bust 1987), mini halos (Rees 1986), caustics in velocity space (McGill 1990), and other scenarios. Recent numerical simulations have, however, shown that the physical condition is a mixture of many such scenarios (Cen et al.1994, Hernquist et al.1995, Miralda-Escudè et al.1995, Zhang et al.1995). The simulations, performed with a variety of structure formation models, show that transient, pancake-like regions of collapsing objects,— and not necessarily virialized objects—produce most of the Ly α forest lines with $N_{\text{HI}} \lesssim 10^{15} \text{ cm}^{-2}$. For example, Miralda-Escudè et al.(1995) find that the pancake associated with a typical Ly α forest line has a baryonic mass $\sim 10^{10} M_{\odot}$ at $z \sim 3$, with a thickness $\sim 50 - 100 h^{-1} \text{ kpc}$, and a transverse size $\sim 1 \text{ Mpc}$ (where $H = 100 h \text{ km s}^{-1} \text{ Mpc}^{-1}$ is the Hubble constant at present

epoch). The numerical simulations find excellent fits with observations of the H I column density distribution of Ly α lines and the line profiles. (In the simulations, the Lyman limit and damped Ly α systems in general come from lines of sight through denser and more spherical objects.)

That such objects should be prevalent in the universe is not surprising. ‘Zeldovich pancake’ is the inevitable result of the fact that a near simultaneous collapse of an object along all three directions, as in a spherical collapse model, is very unlikely. Zeldovich (1970) pointed out that a one dimensional collapse is more probable to occur. Zeldovich and Sunyaev (1972) then considered the fate of gas inside such a nearly two dimensional pancake, although they considered very large masses ($\sim 10^{13} M_{\odot}$) which are the typical masses of the first collapsing objects in a HDM universe. For a CDM like structure formation model, the first objects to collapse have much smaller masses. Therefore, in such a universe the existence of pancakes with smaller masses is not unexpected.

Such pancakes would have masses several times that of the Jeans mass of the intergalactic medium (IGM). In a photoionized IGM, with temperatures $\bar{T} \sim 10^4$ K, the sound velocity is ~ 15 km s $^{-1}$. The baryonic gas, therefore, does not fall into, and cool to form galaxies in, dark matter potential wells with velocity dispersions smaller than this sound velocity. Recent numerical simulations support this scenario (Thoul and Weinberg 1995). The Jeans mass of the IGM, therefore, sets the mass scale above which the baryonic gas can fall into the dark matter potential well. The Jeans (total) mass is $\sim 5 \times 10^{10} h^{-1} (\bar{T}/10^4)^{1.5} M_{\odot}$ at $z \sim 3$ for such temperatures in the IGM in a $\Omega_o = 1$ universe. This corresponds to a Jeans length of $0.7 (\bar{T}/10^4)^{0.5} h^{-1} (1+z)^{-1.5}$ Mpc. This is basically the length $\approx c_s (1/(G\rho_{CDM})^{0.5})$, where the term inside brackets is the dynamical time of the halo (see, e.g., eqn (5) of Reisenegger and Miralda-Escudè 1995). The (total) masses of the typical first collapsing objects at that redshift would, therefore, be several times this mass scale. It is no wonder then that the baryonic masses of the typical mini pancakes in the numerical simulations are found to be of the order of $10^{10} M_{\odot}$.

In CDM like theories, smaller structures will also form, but due to the non-zero sound velocity of the baryonic gas, the gas will not be clumped in such smaller structures.

The idea of mini pancakes in the context of Ly α lines is also motivated by the recent observations of coincident absorption lines in close quasar pairs. The observed fraction (of $\sim 50 - 80\%$) of coincident lines of two quasar pairs Q0107-025AB and Q1343+266AB, with proper separations of $360h^{-1}$ kpc and $40h^{-1}$ kpc at redshifts $z \sim 1$ and $z \sim 2$ (Dinshaw et al.1994, Dinshaw et al.1995, Bechtold et al.1994), show that the Ly α absorbing systems have transverse sizes of the order of a Mpc. With such large transverse sizes, the systems need to have a small ‘thickness’, *i.e.* the systems need to be flat, so that the total amount of gas in Ly α absorbers do not exceed the limit on Ω_b from Big Bang nucleosynthesis (Rauch and Haehnelt 1995).

Recently Rees (1995) has discussed the possible mass scales of the pancakes associated with Ly α forest lines. He has suggested that mass scales between 10^9 and $10^{12} M_\odot$, with various collapse factors (in the range of $1 - 3$) are enough to cover the range of H I column density of Ly α clouds below those of Lyman limit systems. The present work is aimed towards quantifying these speculations.

Zeldovich and Sunyaev (1972) discussed the behavior of gas in pancakes approximating the initial perturbation that leads to the formation of the pancake as a plane sinusoidal wave. They described the density and temperature profiles of the gas as functions of time. The goal of this work is to pursue the mini pancake model of the Ly α forest lines, along the lines followed by Zeldovich and Sunyaev (1972) for large pancakes. Such an analytical picture will give us the dependences of the various observables on different parameters, which is sometimes difficult to understand from the results of time consuming numerical simulations. The questions asked in this paper relate to the physical conditions in these pancakes, the relation between the mass scale of pancakes and their H I column density, and also the evolution of the pancake gas in short time

scales.

The plan of the paper is as follows. §2 discusses the physical conditions of the pancake gas and determines the density and temperature profile. §3 then calculates the Ly α absorption line profile and discusses the possible signatures of the pancakes in the observed profiles. The different time scales for the pancake gas are then computed in §4, and some of the implications of these results are discussed in §5.

2. GAS IN MINI PANCAKES

2.1. Preliminaries

If the mass of the collapsing object is larger than the current Jeans mass, then the baryonic gas will also collapse with the dark matter. In the Zeldovich approximation, the trajectory of a particle is given by

$$\mathbf{r} = a(t)(\mathbf{q} + b(t)\mathbf{p}(\mathbf{q})) . \quad (1)$$

Here $\mathbf{r}(t, \mathbf{q})$ is the actual position of a particle as a function of its Lagrangian (initial) coordinate \mathbf{q} and time t . The function $\mathbf{p}(\mathbf{q})$ describes the initial perturbation, $a(t)\mathbf{q}$ is due to cosmological expansion, and $a(t)b(t)$ describes the growth of the perturbation in the linear regime. It then follows that, in the linear regime, the growth of the density perturbation in three spatial directions near a particle with a given \mathbf{q} will be given by

$$\begin{aligned} \rho(\mathbf{r}, t) &= \frac{\bar{\rho}(t)}{\det(\delta_{ij} + b(t)(\partial p_j / \partial q_i))} \\ &= \frac{\bar{\rho}(t)}{[1 - b(t)\lambda_1(\mathbf{q})][1 - b(t)\lambda_2(\mathbf{q})][1 - b(t)\lambda_3(\mathbf{q})]} , \\ \delta(\mathbf{r}, t) &\approx b(t)(\lambda_1 + \lambda_2 + \lambda_3) . \end{aligned} \quad (2)$$

Here, $\bar{\rho}(t)$ is the background density of the universe at t , δ is the density contrast, and $-\lambda_1, -\lambda_2, -\lambda_3$ are the eigenvalues of $(\partial p_j / \partial q_i)$. In the generic case, the three eigenvalues will

be different from one another. The probability distribution of the eigenvalues was first derived by Doroshkevich. The probability that $\lambda_1, \lambda_2, \lambda_3$ will all simultaneously be either positive or all negative is ~ 0.08 . The probability that there is contraction in one direction and expansion in other two, is ~ 0.42 .

In the generic case, when the eigenvalues are different from one another, the contraction will be strongest in the direction for which the corresponding eigenvalue is the largest among the three. Eqns (2) show that, the density of the matter around the Lagrangian coordinate \mathbf{q} will diverge and the matter will be compressed to a sheet in the (actual) Eulerian space, when one of the eigenvalues, say, λ_1 , satisfies $b(t)\lambda_1 = 1$. It can be shown that the density profile in the case of one dimensional contraction is given by $\rho \propto r^{-2/3}$ (see, e.g., eq. (2.7) in Zeldovich and Shandarin 1989).

2.2. Gas infall and shock

Although we use the Zeldovich-Sunyaev formalism for mini pancakes, we must note the caveats involved. As mentioned above, mini pancakes are structures with masses just above the Jeans scale and, therefore, gas pressure plays an important role, unlike in the case of large pancakes discussed by ZS72. However, for analytical simplicity, we neglect gas pressure in this work.

For analytical simplicity, it is assumed that $\Omega = 1$. It is also assumed that the gas in the IGM is reionized (and reheated) by the time the mini pancakes form. The intensity of the UV background radiation (at 912 \AA) is written as $J = J_{-21} 10^{-21} \text{ erg s}^{-1} \text{ cm}^{-2} \text{ sr}^{-1} \text{ Hz}^{-1}$. The temperature, \bar{T} , of the IGM gas roughly obeys $\bar{T} \propto (1+z)$ after reheating (Miralda-Escudè and Rees 1994).

The baryonic gas particles will initially follow the dark matter and form a sheet. A shock wave

will soon form which will travel outward. ZS72 (see also Zeldovich and Novikov 1983; Zeldovich and Shandarin 1989) estimated the velocity of the shock by assuming that the initial perturbation is a plane sinusoidal wave. In reality, of course, the perturbation will be more complicated. However, as shown below, the plane wave approximation can be very useful in learning about the nature of the gaseous pancakes.

Pancakes are formed when there is a region in space where the velocity field is coherent. Consider a pancake which is associated with such a region with a length scale of perturbation L , and therefore, with some mass M (the total mass initially contained in the region of perturbation). The perturbation is assumed to be a plane wave with a wavelength equal to λ . (Eqn (A2) in Appendix A shows the relation between the mass and the wavelength.) The derivation of the structure of the pancake using this approximation by ZS72 is briefly described in the Appendix A below (after putting the necessary dependences on h and the baryonic fraction of matter Ω_b ; note that their results are for a $\Omega_b = \Omega = 1$ universe). Since the density of the IGM (Ω_I) is more relevant for the gas inside the pancakes, than the general fraction of baryons in the universe (Ω_b), the former is used in the equations below.

Defining a parameter μ to be the fraction of the total mass M that is inside the region bounded by the shock layers, one can write the velocity with which the gas runs into the matter in the pancake (in the laboratory frame) (eqn (1) in ZS72; (A7) below), as,

$$\begin{aligned} U &= 23.3 h^{1/3} (1 + z_c)^{1/2} (\mu\pi)^{1/2} (\sin(\mu\pi))^{1/2} \left(\frac{M}{10^{11} M_\odot} \right)^{1/3} \text{ km/s}, \\ &\sim 73.3 h^{1/3} (1 + z_c)^{1/2} \left(\frac{M}{10^{11} M_\odot} \right)^{1/3} \mu \text{ km/s}, \quad \mu \ll 1. \end{aligned} \quad (3)$$

Here z_c is the redshift of collapse of the perturbation. It can be shown that (for $\Omega_o = 1$, ZS72; (A5) below)

$$\left(\frac{t}{t_c} \right)^{1/3} = \left(\frac{1 + z_c}{1 + z} \right)^{1/2} = \left(\frac{\sin(\mu\pi)}{\mu\pi} \right)^{-1/2}, \quad (4)$$

where t_c corresponds to z_c . For $\mu \ll 1$, $\mu = \frac{2}{\pi}((t/t_c) - 1)^{1/2}$. The curve for eqn (4) and the above

approximation are plotted in Fig. 1 for $z_c = 3$ and $z_c = 4$. (It is shown below in §4 that the gravitational time scale of mini pancakes limit the possible values of μ to be $\lesssim 0.5$.) Therefore, μ can be used as a parameter equivalent to time t .

The velocity of the gas inside the shock front is assumed to be zero here, as it is expected to be small (see Bond et al.1984). The velocity of the shock front is then given by, $V_{sh} = (1/3)U$ (Jones et al.1981, Bond et al.1984). Note that $U \approx V_{sh}$ in ZS72.

For small values of μ , the (particle) gas density in front of the shock is (eqn (3) in ZS72; (A6) below),

$$\begin{aligned} n_1 &\approx 3n_o \frac{(1+z_c)^3}{\pi^2 \mu^2}, & \mu \ll 1, \\ &= 2.3 \times 10^{-7} h^{-2} (1+z_c)^3 \mu^{-2} \left(\frac{\Omega_I}{0.01} \right), \end{aligned} \quad (5)$$

where it is assumed that the IGM gas is ionized ($\rho = 0.6 n m_p$) and n_o is the particle density at present epoch. The postshock gas density is $n_{sh} = 4n_1$, for a strong shock. The postshock temperature is, again for small μ ,

$$T_{sh} = \frac{0.6 m_p U^2}{3k} = 1.3 \times 10^5 h^{2/3} (1+z_c) \left(\frac{M}{10^{11} M_\odot} \right)^{2/3} \mu^2 \text{ K}. \quad (6)$$

The pressure behind the shock front ($p_{sh} = (4/3) \rho_1 U^2$) is independent of μ (i.e., of how much of matter is inside the shocked layer for a given pancake) for small μ (ZS72).

The distance of the shock front from the central plane of the pancake can be estimated as,

$$\begin{aligned} r_{sh} &= \int V_{sh} dt = \int V_{sh} \frac{dt}{d\mu} d\mu \\ &\approx 0.27 h^{-2/3} (1+z_c)^{-1} \left(\frac{M}{10^{11} M_\odot} \right)^{1/3} \mu^3 \text{ Mpc}, & \mu \ll 1. \end{aligned} \quad (7)$$

As mentioned above and explained in the Appendix, the above expressions are obtained in the absence of gas pressure. As gas pressure is more important for mini pancakes than the large pancakes studied by ZS72, these expressions are only very approximate.

2.3. Density and temperature profile

What is the maximum gas density in the pancake? The maximum density would be infinite for infinite cooling rate and for a zero pressure gas outside, neither of which is true in the present case. It can be shown that the cooling time scale of the gas in the presence of the UV background is larger than the Hubble time at $z \sim 3$ for the relevant gas densities of this problem (see Appendix B).

However, the heating time scale becomes comparable to or shorter than the Hubble time for $z_c \sim 3$ (Appendix B). In the following, we restrict our analysis to $z_c \sim 3$ where both cooling and heating time scales are larger than the Hubble time and assume that the gas contracts adiabatically.

Furthermore, since the evolution of the IGM temperature \bar{T} depends on various parameters and models of ionization (Miralda-Escudè and Rees 1994), we will, for simplicity, assume a constant IGM temperature of $\bar{T} \approx 10^4$ K in the following. Introducing an evolution of \bar{T} will introduce more free parameters, which we will avoid.

If the ambient IGM density is \bar{n} , with pressure \bar{p} (and temperature \bar{T}), then the maximum gas density and temperature in the pancake is given by

$$\begin{aligned} n_{max} &= \bar{n} \left(\frac{p_{sh}}{\bar{p}} \right)^{3/5} = 1.2 \times 10^{-4} h^{12/5} \left(\frac{1+z_c}{4} \right)^{18/5} \left(\frac{M}{10^{11} M_\odot} \right)^{2/5} \left(\frac{\Omega_I}{0.01} \right) \left(\frac{\bar{T}}{10^4 \text{ K}} \right)^{-3/5}, \\ T_{max} &= \bar{T} \left(\frac{n_{max}}{\bar{n}} \right)^{2/3} = 4.7 \times 10^4 h^{4/15} \left(\frac{1+z_c}{4} \right)^{2/5} \left(\frac{M}{10^{11} M_\odot} \right)^{4/15} \left(\frac{\bar{T}}{10^4 \text{ K}} \right)^{3/5} \end{aligned} \quad (8)$$

As mentioned in §2.1, in the Zeldovich approximation, the density of the gas has a profile (in the direction perpendicular to the pancake) that is given by $\rho \propto r^{-2/3}$ (e.g., eqn. (2.7) of Zeldovich and Shandarin 1989). The density profile of the gas can, therefore, be divided into four characteristic regions: (a) in front of the shock, the density follows a $r^{-2/3}$ profile, as explained above; (b) the density jumps by a factor of 4 at the shock front; (c) behind the shock, the gas

again follows a $r^{-2/3}$ profile, in the Zeldovich approximation, as explained above; (d) and then it reaches a maximum when the density is n_{max} of eqn (8). For analytical simplicity, we assume this central region, say, $r < r_o$, with $n \sim n_{max}$ to be a region of uniform density.

In the single wave approximation used here, we have neglected the motion of the gas in the directions along the pancake. In reality, gas will also move along the pancake. Modelling this effect is, however, beyond the scope of the single wave approximation. We neglect it here, and assume that the density in the central region is a constant in time, for the short time evolution we are interested in here ($\mu \ll 1$). Gas will also tend to expand in the perpendicular direction, but for small μ (which is considered in the present work), pressure behind the shock p_{sh} , stays constant with μ (that is, in time) and the ram pressure will tend to confine the gas. In other words, we assume that,

$$\begin{aligned}
 n &\sim n_{max} & r < r_o \\
 &\propto n_{max} \left(\frac{r}{r_o}\right)^{-2/3} & r_o < r < r_{sh} \\
 &\sim n_{sh} & r \sim r_{sh} \\
 &\propto \frac{n_{sh}}{4} \left(\frac{r}{r_{sh}}\right)^{-2/3} & r > r_{sh}.
 \end{aligned} \tag{9}$$

If $r_{sh} < r_o$, then $n \sim n_{max}$, $r < r_{sh}$, and $n \propto \frac{n_{sh}}{4} \left(\frac{r}{r_{sh}}\right)^{-2/3}$ for $r > r_{sh}$. Matching the densities at the various boundaries, as explained above, one obtains for the extent of this central region, as

$$r_o = 3h^{-19/15} \left(\frac{1+z_c}{4}\right)^{-19/10} \left(\frac{M}{10^{11} M_\odot}\right)^{-4/15} \text{ kpc}. \tag{10}$$

This length scale will be important in calculating the column densities in §2.4.

Similarly, the temperature has a maximum value in the central region, as given in eqn (9). At the current position of the shock, r_{sh} , the temperature will be given by eqn (6). For $r_o < r < r_{sh}$, the gas would have been shocked and would be raised to corresponding T_{sh} . As $T_{sh} \propto \mu^2$ and $r_{sh} \propto \mu^3$, it is easy to see that $T \propto r^{2/3}$ for $r_o < r < r_{sh}$. Outside r_{sh} , the temperature the same as

that of the IGM (\bar{T}). We remark here that the temperature profile will in general change in time due to cooling. As explained above, the cooling rate is small for $z \gtrsim 3$ and the above temperature and density profiles hold only in that regime.

The profiles of $\delta = n/\bar{n}$, $\delta_{HI} = n_{HI}/\bar{n}_{HI}$ and T/\bar{T} for a typical pancake are shown in Fig. 2, for $\mu = 0.3, 0.4$. We have used $M = 5 \times 10^{11} M_{\odot}$, $h = 0.75$, $z_c = 3$ and $\Omega_I = 0.03$. For each value of μ , the values of r_o and r_{sh} are first evaluated (eqns (7) and (10)), and then the density at each point in space using eqns (5) and (8). The density of neutral hydrogen is evaluated at each point of the pancake using ionization balance (see §2.4). The increase in the overdensity at later times is due to the decrease in the ambient density in the universe in time. It is seen that the gas in the pancakes have a typical maximum overdensity of order ~ 10 –50 (see also Miralda-Escudè et al.1995). One should note that in reality gas will expand along the pancake, thereby decreasing the central density. Therefore, the overdensity obtained above should be taken as an upper limit.

The density and temperature profiles in Fig. 2 are much different from those in large, massive pancakes, as studied by ZS72, in that the maximum density in their case is much larger, and therefore, r_o is smaller (it was small enough to be unimportant for those pancakes). Also, T_{max} in ZS72 was much lower because a cold IGM gas was assumed. For small μ , the temperature profile does not have the usual ‘double horn’ profile that is expected in large pancakes (Jones, Palmer and Wyse 1981). Such a profile is possible if, $\mu \gtrsim 0.3 h^{-3/15} ((1 + z_c)/4)^{7/10} (M/10^{11} M_{\odot})^{3/15} (\bar{T}/10^4 K)^{1/2}$. As discussed below, large values of μ in general correspond to large N_{HI} . Therefore, such temperature profiles are not expected for small H I column density Ly α lines. The spectra and the corresponding density and temperature profiles obtained in the numerical simulations of Miralda-Escudè et al.(1995) support this.

The extent, or the thickness, of the pancake can be estimated by finding the distance r' where the density contrast $\delta = (n - \bar{n})/\bar{n}$ (where \bar{n} is the background IGM density) is unity. For the

above profile, this happens at $r' \sim (\frac{2\pi^2\mu^2}{3})^{-3/2} r_{sh} \sim 6.2 \times 10^{-2} \mu^{-3} r_{sh}$. For $M = 3 \times 10^{11} M_\odot$ (corresponding to $M_b \sim 10^{10} M_\odot$, for $\Omega_I \sim 0.03$), $h = 0.5$ and $z_c = 3$, the ‘thickness’ of the pancake is ~ 20 kpc. For comparison, the typical thickness for pancakes as reported by Miralda-Escudè et al.(1995) is $50 - 100 h^{-1}$ kpc. It should be noted that this is also consistent with the upper limit on the thickness (~ 50 kpc) put from the combined knowledge of the large transverse sizes of Ly α absorption systems and the value of Ω_b from Big Bang nucleosynthesis (Haehnelt and Rauch 1995).

2.4. Neutral and H I column density

For a line of sight which is perpendicular to the pancake, the total column density of the gas is,

$$\begin{aligned} N_H &\sim 2 \int_{r=0}^{r=r_{sh}} n(r) dr = 2 n_{max} r_o \left\{ 1 + 8.8 h^{1/5} \left(\frac{1+z_c}{4} \right)^{3/10} \left(\frac{M}{10^{11} M_\odot} \right)^{1/5} \mu \right\} \\ &\approx 2.3 \times 10^{18} \left(\frac{\mu}{0.3} \right) \left(\frac{h}{0.5} \right)^{4/3} \left(\frac{1+z_c}{4} \right)^2 \left(\frac{M}{10^{11} M_\odot} \right)^{1/3} \left(\frac{\Omega_I}{0.01} \right) \text{ cm}^{-2}. \end{aligned} \quad (11)$$

This is comparable to the values of column density plotted in Fig. 9a of Miralda-Escudè et al.(1995). For a gas in ionization equilibrium with photoionization by the UV background radiation, and with collisional ionization, one can also estimate the H I column density. Photoionization and recombination rates are taken from Black (1981), and Cen (1992). Fig. 3 (a) and (b) plot N_{HI} and N_H vs. the mass (total and baryonic) that corresponds to the pancake, for a line of sight perpendicular to the pancake. Here $M_b = \mu \Omega_I M$. Fig 3 (c) plots N_H against N_{HI} . Fig. 3 (d) shows the evolution of N_{HI} in time, or equivalently, with increasing values of μ .

The plots show that, in general, larger (more massive) pancakes correspond to higher N_{HI} (approximately, $N_{\text{HI}} \propto M^{2/3}$ (see below in §4 for a discussion on this). There is however a scatter, due to possible differences in the ambient density (Ω_I), collapsing redshift (z_c), and due to the evolution of pancakes in time. Since $N_H \propto \Omega_I$, for a photoionized gas, $N_{\text{HI}} \propto \Omega_I^2$ (see below).

The column density increases at higher collapse redshifts, but this can be an artifact of the assumption that a constant background temperature (\bar{T}). In reality, \bar{T} may increase with redshift (in a photoionized universe $\bar{T} \propto (1+z)$ much after the reheating epoch). This will decrease the density in the central region and will decrease the column density. Such an evolution in the IGM temperature introduces another parameter for the pancakes, and will not be discussed here to avoid confusion. The evolution of the individual pancakes first increases N_{HI} till about $\mu \sim 3$ (for $M \gtrsim 10^{11} M_{\odot}$), after which hotter temperatures deplete more neutral atoms and halts the increase in N_{HI} .

This behavior is also reflected in Fig. 3(c) which plots N_H against N_{HI} . Large values of N_{HI} are either associated with large M or large μ , both of which are associated with high temperature, which tends to decrease the neutral fraction. This fact, therefore, puts an upper limit on the value of N_{HI} for Ly α lines from pancakes. In particular, for $J_{-21} = 1$ and $\Omega_I \sim 0.03$, mini pancakes can only give rise to Ly α lines with $N_{\text{HI}} \lesssim 10^{14} \text{ cm}^{-2}$ for $z_c = 3$. For $z_c = 4$, this limiting value is found to be $N_{\text{HI}} \lesssim 10^{14.5} \text{ cm}^{-2}$.

3. ABSORPTION LINES

Armed with the knowledge of the density and temperature profiles, one can calculate the Ly α absorption line profile for a line of sight through the pancake. The additional information necessary is that of the velocity field. The bulk velocity of the gas within the shocked layers is small and is neglected here. Outside the shocked layer, the gas particles stream towards the pancake with velocity that is determined by the initial velocity perturbation. In Zeldovich approximation, the velocity of a particle remains constant. This allows one to find the velocity profile of the gas at later times.

Consider a particle initially at Lagrangian (comoving) coordinate ξ with velocity v . This

particle will eventually meet the shock front with the same velocity v at some point r in the Eulerian (physical) coordinate. This velocity v and the point r are given by eqns (3) and (7). Also, as described in Appendix, every point ξ is associated with a value of μ . Since the velocity remains constant, this mapping is also true for other points in physical space. For any other point r' , one needs to find the corresponding ξ' or μ' from eqn (7) and then find the velocity from eqn (3).

Let $r = 0$ be the origin (in the dimension perpendicular to the pancake) at some redshift z . The total velocity of a particle at r is therefore, $V(r) = Hr + v(r)$ where H is the Hubble constant at z and $v(r)$ is the peculiar velocity. The profile of the absorption line is determined by the overdensity of H I in velocity space, convolved with a Gaussian of width $b(r) = \{2kT(r)/m_p\}^{0.5}$. The smoothed H I overdensity at some velocity V' in velocity space is given by (Miralda-Escudè and Rees 1992),

$$\delta_{\text{HI}}(V') = \int dr \delta_{\text{HI}}(r) H \exp\left(-\frac{(V(r) - V')^2}{b(r)^2}\right) (\pi^{1/2} b(r)). \quad (12)$$

If the Gunn-Peterson optical depth to Ly α absorption by the IGM is τ_{GP} , then the total optical depth at velocity V' is given by $\tau(V') = \tau_{GP}(1 + \delta_{\text{HI}}(V'))$. Here, τ_{GP} is the Gunn-Peterson opacity, and in a photoionized universe it is given by $\tau_{GP} = 0.32 \Omega_I^2 h^3 (1+z)^{4.5} J_{-21}^{-1}$ (using eqn (39) of Miralda-Escudè and Ostriker (1990), with clumping factor $f = 1$ and the spectral index $\alpha = 1$).

Examples of line profiles are plotted in Fig. 4, for various values of μ for a particular pancake, and for different orientations. Also shown are the fits to the profiles using Voigt function, which depend on N_{HI} and a b parameter. The value of N_{HI} changes when the angle of inclination (θ) of the pancake to the line of sight is changed, and is roughly proportional to $(\cos(\theta))$. (The total H I column density is exactly proportional to $(\cos(\theta))$, but this is only approximately true for the H I column density of the fitted central line, as some of the neutral atoms also show up in the extra lines.) This is mainly because of our assumed flat density profile for $r \lesssim r_o$.

It is seen that the absorption lines from pancake can be fit by Voigt profiles, although with

some deviations. In general, the absorption profile consists of a central dip, which follows a Voigt profile, and some extra dips which are shifted from the central one in frequency space. These wings make the value of N_{HI} from fitting the central portion of the profile smaller than the corresponding value from Fig. 3 (d). Absorptions by some neutral atoms show up in the profiles away from the central portion – causing the absorption profile to deviate from the Voigt profile.

Even though pancakes are associated with bulk motions, the thermal gas makes the profile close to Voigt profile for lines with large N_{HI} . Lines with small N_{HI} , however, are in general associated with small values of μ , when only a small fraction of the total mass has been heated through adiabatic compression. One, therefore, expects to see the deviations from a simple Voigt profile in the case of low mass pancakes, or when μ is small in a pancake, when bulk motion dominates over the thermal contribution to b . Such an example is shown in Fig. 4(d). It is similar to some of the low column density lines in the spectra obtained in the numerical simulations of Miralda-Escudè et al.(1995) (see their discussion in §3.3.3).

The deviation of the absorption profile from a Voigt profile can be quantified by the ratio of the equivalent width of the central dip with the Voigt profile (W_c) to the total equivalent width in the absorption profile (W_{tot}). As shown in Fig. 5a, this ratio is very small for lines with small total equivalent widths. These lines are produced by less massive pancakes and for pancakes with small values of μ (and therefore with smaller values of N_{HI}). The curves show that a fraction of $\gtrsim 0.1$ of the total equivalent width of the absorption line shows up in the wings. The wings could, however, be fitted separately as extra lines with Voigt profiles, but the interpretation of these (small N_{HI}) lines as separate ‘objects’ or ‘clouds’ would not be appropriate, as these extra lines simply reflect the bulk motion in the pancake (see also Rauch 1995). For $M \gtrsim 5 \times 10^{11} M_{\odot}$, the ratio $W_c/W_{tot} \lesssim 0.5$ for $W_{tot} \lesssim 0.1 A$, corresponding to $N_{\text{HI}} \lesssim 2 \times 10^{13} \text{ cm}^{-2}$. Several of the observed small N_{HI} ($N_{\text{HI}} \lesssim 10^{13} \text{ cm}^{-2}$) lines, therefore, reflect the bulk motions relevant for the formation of mini pancakes (see also McGill 1990, where it was pointed out that velocity cusps in

redshift space can masquerade as Ly α lines).

For small deviations from the Voigt profile, the b value of the central line is determined by thermal motion of the atoms. Fig 5b plots the ratio of the b from Voigt profile fitting of the central line, to the b that corresponds to T_{max} of eqn (6), as a function of N_{HI} of the central line (determined from profile fitting). It clearly shows that for lines with $N_{\text{HI}} \gtrsim 10^{13} \text{ cm}^{-2}$, the b value is determined by the thermal motion of the atoms. For lines with $N_{\text{HI}} \gtrsim 10^{14} \text{ cm}^{-2}$, however, the temperature in the shock front dictates the value of b (and therefore deviates from the value of b corresponding to T_{max} of the central region). A statistical study for the distribution of b is, however, beyond the scope of the present work.

4. DISCUSSIONS

In CDM type scenarios the mass scale of the first gaseous pancakes is given by the Jeans mass. The cutoff in the power spectrum, however, is not as sharp as the lower cutoff in HDM scenarios. Also, the power spectrum in the vicinity of the Jeans cutoff is flatter for CDM type structure formation models than the HDM power spectrum. This means that the masses of the first gaseous pancakes may not have a single value and is likely to have a distribution.

It is not clear whether or not the column density distribution of Ly α lines arises from this distribution in mass. If that is the case, then the above relation can be used, in principle, to calculate the distribution of N_{HI} (number of lines with H I column density N_{HI} per unit H I column density per unit redshift, or $(dN/dN_{\text{HI}} dz)$), if an expression for the distribution function of the pancakes can be found in terms of their masses (or, equivalently, the length scale L of the region in which the initial velocity field is coherent). However, the cause of the column density distribution of Ly α lines is likely to be more complicated than this. Firstly, if the pancakes survive for about a Hubble time, the evolution of the pancakes need to be taken into account. In any case, such a

statistical study is beyond the scope of this work.

Several observations involving double lines of sight suggest that the sizes of regions in the direction perpendicular to the line of sight can be several hundreds of kpc. Miralda-Escudè et al.(1995) find the typical transverse size of pancakes to be ~ 1 Mpc. As mentioned earlier, the Jeans scale at $z \sim 3$ is $\lambda_J \sim 0.13 (\bar{T}/10^4 K)^{0.5} (h/0.75)^{-1} ((1+z)/4)^{-1.5}$ Mpc, for a photoionized universe with $\bar{T} \propto (1+z)$. The typical first pancakes with infalling baryonic gas will therefore have sizes several times this (the diameter will be twice this value). It is, therefore, conceivable that the transverse size of pancakes would be ~ 1 Mpc. More over, the gas flows in the transverse direction will make the size even larger. As mentioned earlier, when one of the eigenvalues ($\lambda_1, \lambda_2, \lambda_3$) is negative (which describes contraction), the probability that the other two eigenvalues are positive (that is gas *expands* in the transverse direction), is ~ 0.42 (ZS72). As suggested by many previous authors, this expansion can make the pancakes larger in the transverse direction, and increase the probability of detection.

Finally, a word about the approximation used is in order. The results obtained here should be considered as only very approximate, and have large error bars, because of the approximation of single plane waves. However, it is interesting that some information about the behaviour of the gas in pancakes, and the effects on the absorption profile, can still be obtained from such simple approximations.

5. CONCLUSIONS

In this paper, mini pancakes are analytically modeled with single plane wave perturbations, and the consequences for the Ly α absorption lines from these mini pancakes are discussed. Although a very crude approximation to the real pancakes, this model is shown to elucidate a number of important points. The most important results of the paper are contained in Figs. 3

and 5. They show the mass scales of pancakes that corresponds to the HI column densities of Ly α forest lines with $N_{\text{HI}} \lesssim 10^{14.5} \text{ cm}^{-2}$, the evolution of N_{HI} in time for different pancakes, and the importance of bulk motions in low equivalent width absorption lines. It is shown that pancakes with total masses in the range of $M \sim 10^{11}\text{--}10^{12} M_{\odot}$ (and a baryonic mass of $M_b \sim 10^{9.5}\text{--}10^{10.5} M_{\odot}$) can give rise to Ly α lines with $N_{\text{HI}} \lesssim 10^{14.5} \text{ cm}^{-2}$. Here, the mass corresponds to the size of the perturbation. These structures have an overdensity of the order of ~ 10 . Also, there is a maximum value of N_{HI} for a given value of Ω_I . For $J_{-21} = 1$, a temperature of the IGM of $\bar{T} = 10^4$ K, and $\Omega_I \sim 0.03$, mini pancakes only give rise to Ly α lines with $N_{\text{HI}} \lesssim 10^{14.5} \text{ cm}^{-2}$. These results hold only for $z_c \sim 3$ for which the gas in the mini pancake can be assumed to be compressed adiabatically.

Calculating the expected absorption profiles from the pancakes, we also confirm that the information of the bulk motion associated with pancakes is carried by low HI column density lines with $N_{\text{HI}} \lesssim 10^{13} \text{ cm}^{-2}$. The lines in general consist of a central dip with wings that signify bulk motions. The wings are most significant for low equivalent width lines. The lines could be fitted with more than one Voigt profiles, but would not necessarily mean that the lines arise in separate, discrete objects.

I am grateful to my colleagues in IUCAA and Dr. K. Subramanian for valuable discussions, encouragement and criticisms. I also thank the anonymous referee whose comments have improved the manuscript. I am indebted to Prof. P. J. E. Peebles for an inspiring discussion on Ly α lines and pancakes.

REFERENCES

- Bechtold, J., Crotts, A. P. S., Duncan, R. S., Fang, Y. 1994, *ApJ*, 437, L83
- Black, J. H. 1981, *MNRAS*, 197, 553
- Bond, J. R., Centrella, J., Szalay, A. S., & Wilson, J. R. 1984, *MNRAS*, 210, 515
- Cen, R., Miralda-Escudè, J., Ostriker, J. P., & Rauch, M. 1994, *ApJ*, 437, L9
- Cen, R. 1992, *ApJS*, 78, 341
- Dinshaw, N., Impey, C. D., Foltz, C. B., Weymann, R. J., Chaffee, F. H. 1994, *ApJ*, 437, L87
- Dinshaw, N., Foltz, C. B., Impey, C. D., Weymann, R. J., Morris, S. L. 1995, *Nature*, 373, 232
- Hernquist, L., Katz, N., Weinberg, D. H., & Miralda-Escudè, J. 1995, *ApJ*, 457, L51
- Jones, B. J. T., Palmer, P. L., & Wyse, R. F. G. 1981, *MNRAS*, 197, 967
- McGill, C. 1990, *MNRAS*, 242, 544
- Miralda-Escudè, J. & Ostriker, J. P. 1990, *ApJ*, 350, 1
- Miralda-Escudè, J. & Rees, M. J. 1993, *MNRAS*, 260, 617
- Miralda-Escudè, J. & Rees, M. J. 1994, *MNRAS*, 266, 343
- Miralda-Escudè, J., Cen, R., Ostriker, J. P., & Rauch, M. 1995, *ApJ* Submitted (astro-ph/9511013)
- Ostriker, J. P., & Ikeuchi, S. 1983, *ApJ*, 268, L63
- Rauch, M., & Haehnelt, M. C. 1995, *MNRAS*, 275, L76
- Rauch, M. 1996, in *Cold Gas at High Redshift*; in press (astro-ph/9512002)
- Rees, M. J. 1986, *MNRAS*, 218, 25p
- Rees, M. J. 1995, in *QSO Absorption lines*, Proc. ESO Workshop, ed. G. Meylan (Heidelberg: Springer); p. 419
- Reisenegger, A., & Miralda-Escudè, J. 1995, *ApJ*, 449, 476

Sargent, W. L. W., Young, P. J., Boksenberg, A. & Tytler, D. 1980, *ApJS*, 42, 41

Thoul, A., & Weinberg, D. 1995, *ApJ*, 442, 480

Vishniac, E. T., & Bust, G. S. 1987, *ApJ*, 319, 14

Zeldovich, Ya. B. 1970, *A&A*, 5, 84

Zeldovich, Ya. B., & Novikov, I. D. 1983, *The Structure and Evolution of the Universe* (University of Chicago, Chicago/London)

Zeldovich, Ya. B., & Shandarin, S. 1989, *Rev. Mod. Phys.*, 61, 185

Zeldovich, Ya. B., & Sunyaev, R. A. 1972, *A&A*, 20, 189 (ZS72)

Zhang, Y., Anninos, P., & Norman, M. 1995, *ApJ* Submitted

Figure captions Fig. 1 – The parameter μ is plotted against redshift z for two different collapse redshifts $z_c = 3, 4$. Solid curve is the result of eqn (4) and the dashed curve corresponds to the approximation used in the work.

Fig. 2 – (a) Curves show the overdensity profile of pancakes with $M = 5 \times 10^{11} M_\odot$ at $\mu = 0.3$ (solid curve) and at $\mu = 0.4$ (dotted curve). Most of the increase in the overdensity in time comes from the decrease in the ambient density.

(b) Similar curves for H I overdensity profile.

(c) Curves for the temperature profile for the same parameters. The temperature of the IGM gas, $\bar{T} = 10^4$ K.

Fig. 3 – (a) The H I column densities N_{HI} of pancakes, for regions where the H I overdensity is greater than unity, are plotted against the total mass M of the pancakes for lines of sight perpendicular to the pancake. Dotted, short dashed and long dashed curves refer to pancakes with $\mu = 0.2, 0.3, 0.4$ respectively, for $\Omega_I = 0.03$. The collapse redshift of the pancakes $z_c = 3$.

(b) Same as in Fig. 3(a), except that N_{HI} is plotted against the baryonic masses $M_b = \mu \Omega_I M$. The upper set of curves correspond to collapse redshift $z_c = 4$ and the lower set, to $z_c = 3$.

(c) Total column density N_H is plotted against N_{HI} for $\mu = 0.2, 0.3, 0.4$, $\Omega_I = 0.03$, $z_c = 3$.

(d) The H I column densities N_{HI} of different masses are plotted as functions of μ (or, equivalently, time). From top to bottom, the masses involved are $M = (50, 10, 5, 1) \times 10^{11} M_\odot$. The dotted curve shows the contour left of which the total equivalent width W_{tot} of the corresponding Ly α absorption profile is less than $0.1 A$.

Fig. 4 – (a) The Ly α absorption profile for a pancake with $M = 5 \times 10^{11} M_{\odot}$, $\mu = 0.3$ for a line of sight perpendicular to the pancake, for $z_c = 3.$, $h = 0.75$, $\Omega_I = 0.03$. The Voigt profile fitted to the central dip has $N_{\text{HI}} = 2.4 \times 10^{13} \text{ cm}^{-2}$ and $b = 35 \text{ km/s}$.

(b) The profile for the same pancake but with $\mu = 0.4$. The Voigt profile has $N_{\text{HI}} = 10^{14}$ and $b = 35 \text{ km/s}$.

(c) The profile for the same pancake with $\mu = 0.3$ but for a line of sight making an angle 45° to the pancake. The Voigt profile fitted has $N_{\text{HI}} = 3.4 \times 10^{13} \text{ cm}^{-2}$ and $b \sim 35 \text{ km/s}$.

(d) The profile for a pancake with $M = 10^{11} \text{ cm}^{-2}$ at $\mu = 0.25$ (the cosmological parameters remain the same). The Voigt profile fitted to the central dip has $N_{\text{HI}} = 3.6 \times 10^{12} \text{ cm}^{-2}$ and $b = 30 \text{ km/s}$.

Fig. 5 – (a) The ratio of the equivalent width of the fit to the central dip W_c to the total equivalent width of the absorption profile W_{tot} is plotted against W_{tot} for different masses. Curves with long dash, short dash and solid line correspond to $M = 10^{11}, 5 \times 10^{11}, 10^{12} M_{\odot}$ with $h = 0.75$, $z_c = 3$ and $\Omega_I = 0.03$.

(b) The ratio of the b value of the Voigt fit to the central line to the b corresponding to T_{max} of the pancake is plotted against the values of corresponding N_{HI} of the central line. The cosmological parameters are the same as in Fig. 5(a).

Fig. B – The heating and cooling rate of gas with density $n_H = 10^{-4} \text{ cm}^{-3}$ in the presence of a photoionizing background of intensity $J_{-21} = 1$ are plotted as functions of the temperature. The upper solid curve is the cooling rate for $J_{-21} = 0$. The solid line at bottom is the cooling rate for $J_{-21} = 1$ and the dashed line is the heating rate for the same ionizing background.

A. APPENDIX A

The derivations of eqns (3), (4), and (5) are sketched briefly below, following ZS72 (see also Zeldovich and Novikov 1983). The perturbation leading to the formation of the pancake is assumed to be a sinusoidal plane wave in an $\Omega = 1$ universe, with baryon fraction Ω_b . The motion of particles in the direction of contraction (before being compressed by shock waves) is given by

$$r = t^{2/3}\xi - bt^{4/3} \sin k\xi . \quad (\text{A1})$$

Here ξ is the Lagrangian coordinate. The mass M that is contained in the region (of comoving length scale λ) of perturbation is given by,

$$M = \bar{\rho} \left(\frac{\lambda}{2}\right)^3 = \rho_o \left(\frac{\lambda(1+z)}{2}\right)^3 ; \bar{\rho} = \frac{1}{6\pi Gt^2} ; \lambda = \frac{2\pi t^{2/3}}{k} . \quad (\text{A2})$$

Here, $\rho_o = 1.89 \times 10^{29} h^2 \Omega_I$ is the present day mass density of the IGM. For matter not yet compressed by the wave, the density is given by

$$\rho = \frac{1}{6\pi Gt^2} \frac{1}{1 - bt^{2/3}k \cos k\xi} . \quad (\text{A3})$$

Therefore, t_c , the epoch of the formation of the pancake at $r = 0$ is determined by $kbt_c^{2/3} = 1$. The parameter μ is then defined as $\mu = \frac{k\xi}{\pi}$. This means that the interval $0 < \xi < \pi/k$ in the Lagrangian coordinate is equivalent to $0 < \mu < 1$.

If the pressure of the IGM gas is assumed to be zero, then a plane at $r = 0$ reaches infinite density. One can think of a wave front in the Lagrangian coordinate corresponding to the particles reaching this plane. This wave front moves outward, and the Lagrangian coordinate μ_1 of the wave front is given by,

$$r = 0 = \pi\mu_1 - (bkt_c^{2/3}) \left(\frac{t}{t_c}\right)^{2/3} \sin \pi\mu_1 . \quad (\text{A4})$$

Note that, in reality the shock will form at a distance from the $r = 0$ plane, and the above expression, which assumes an origin at $r = 0$ is reasonable only for small gas pressure. However,

as explained in the text, we neglect gas pressure in the present work. This shows that,

$$\left(\frac{t}{t_c}\right)^{2/3} = \left(\frac{\pi\mu_1}{\sin \pi\mu_1}\right). \quad (\text{A5})$$

Using (A3), the density at the front is then given by,

$$\begin{aligned} \rho_1 &= \frac{\bar{\rho}}{1 - \left(\frac{t}{t_c}\right)^{2/3} \cos \pi\mu_1} \\ &= \frac{\bar{\rho}}{1 - \frac{\pi\mu_1}{\tan \pi\mu_1}} \\ &= \rho_o \frac{(1+z)^3 (\sin \pi\mu_1 / \pi\mu_1)^3}{(1 - \pi\mu_1 / \tan \pi\mu_1)} \\ &\sim 3\rho_o \frac{(1+z)^3}{\pi^2 \mu_1^2}, \quad \mu_1 \ll 1. \end{aligned} \quad (\text{A6})$$

The velocity of matter running into the wavefront is obtained as, (for small $k\xi$ and for $t \sim t_c$, *i.e.*, $\mu \ll 1$) as,

$$\begin{aligned} U_1 = -\frac{dr}{dt} &\approx \frac{2}{3} \frac{\xi}{t^{1/3}} - \frac{4}{3} b t^{1/3} k \xi \\ &= \frac{2}{3} \frac{\xi}{t^{1/3}} - \frac{4}{3} \left(\frac{t}{t_c}\right)^{1/3} \frac{\xi}{t_c^{1/3}} \\ &\sim \frac{2}{3} \left(\frac{t}{t_c}\right)^{1/3} \frac{\xi}{t^{1/3}} \\ &= \frac{2}{3} \frac{1}{t} \frac{t^{2/3}}{k} (k\xi) \\ &\approx \frac{2}{3} \frac{\lambda}{t} \frac{1}{2\pi} \left(\frac{t}{t_c}\right)^{1/3} (\pi\mu_1)^{1/2} (\sin \pi\mu_1)^{1/2} \\ &= 23.3 h^{1/3} (1+z_c)^{1/2} (\pi\mu_1)^{1/2} (\sin \pi\mu_1)^{1/2} \left(\frac{M}{10^{11} M_\odot}\right)^{1/3} \text{ km/s}. \end{aligned} \quad (\text{A7})$$

Here $(1+z_c)$ corresponds to t_c .

For matter with non-zero pressure, the above equations will remain approximately unchanged for large μ , when the wave has moved a large distance. The central regions will, however, not attain infinite density in this case (see §2.3).

B. APPENDIX B

We present the cooling curve for a gas in the presence of ionizing UV photons here. The cooling processes used in the calculation include collisional ionization, recombination, dielectronic recombination and collisional excitation, in a gas containing hydrogen and helium ($X = 0.76$), as listed in Black (1981). We used the photoionization cross-section for $J_{-21} = 1$ as in Black (1981) (for a spectral index $\alpha = 1$). Figure B shows the cooling rate (solid lines) for a gas with $n_H = 10^{-4} \text{ cm}^{-3}$ with $J_{-21} = 0$ and $J_{-21} = 1$, and shows that line cooling is suppressed by the ionizing photons substantially. For higher densities, the suppression of line cooling is less. Therefore, for a maximum density of $\sim 10^{-4} \text{ cm}^{-3}$ and temperature $\lesssim 10^6 \text{ K}$, as in eqn (8), the cooling rate of the gas is $\sim n_H^2 10^{-24} \sim 10^{-32} \text{ erg cm}^{-3} \text{ s}^{-1}$. This implies a cooling time scale of $10^{17} (T/10^5 \text{ K}) \text{ s}$, which is larger than the Hubble time at $z \sim 3$.

Fig. B also plots the heating rate (dashed line) for the same density and for $J_{-21} = 1$. It is seen that at $T \sim 10^{4.7}$ and $n = 10^{-4} \text{ cm}^{-3}$ (eqn (8)), the heating time scale is $\frac{3/2 nkT}{\Gamma} \sim 3 \times 10^{16} \text{ s}$, comparable to the Hubble time at $z \sim 3$ for a flat universe and $h = 0.75$.

Therefore, the assumption of adiabaticity for the gas in mini pancakes is reasonable only for $z_c \sim 3$.

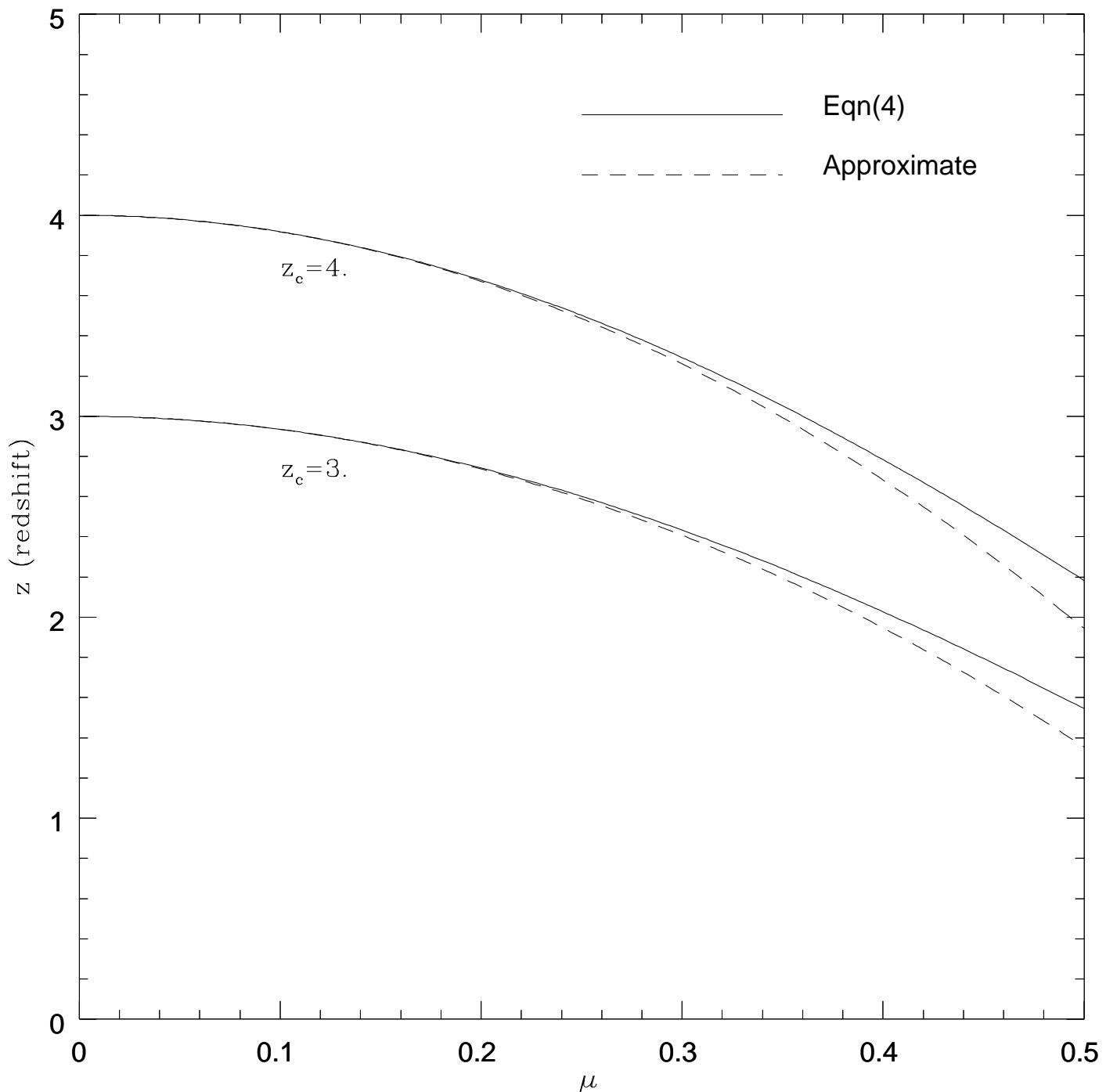


Fig. 1

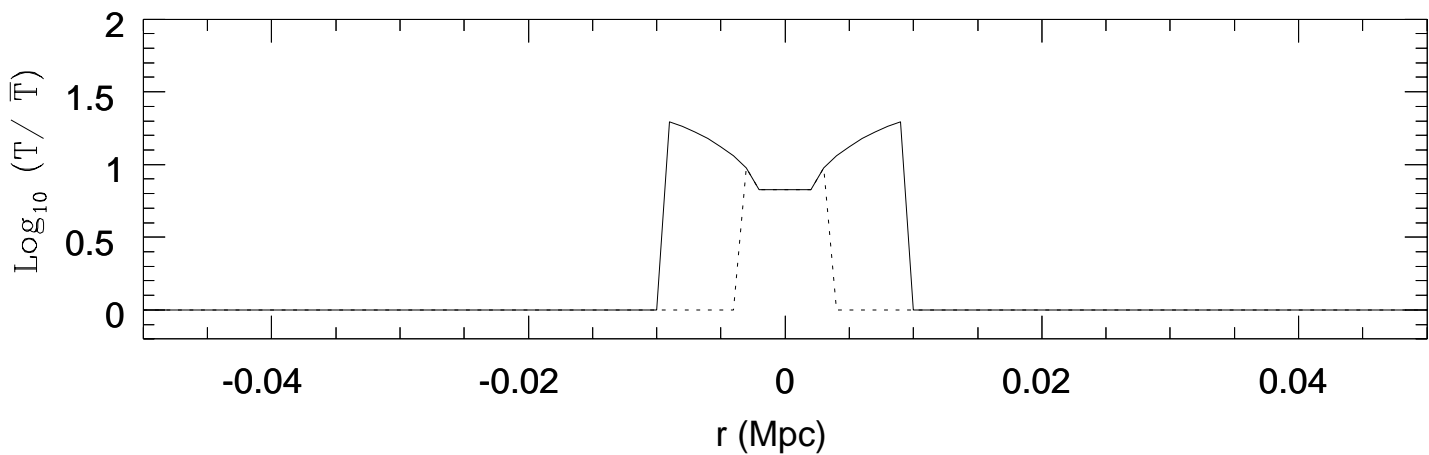
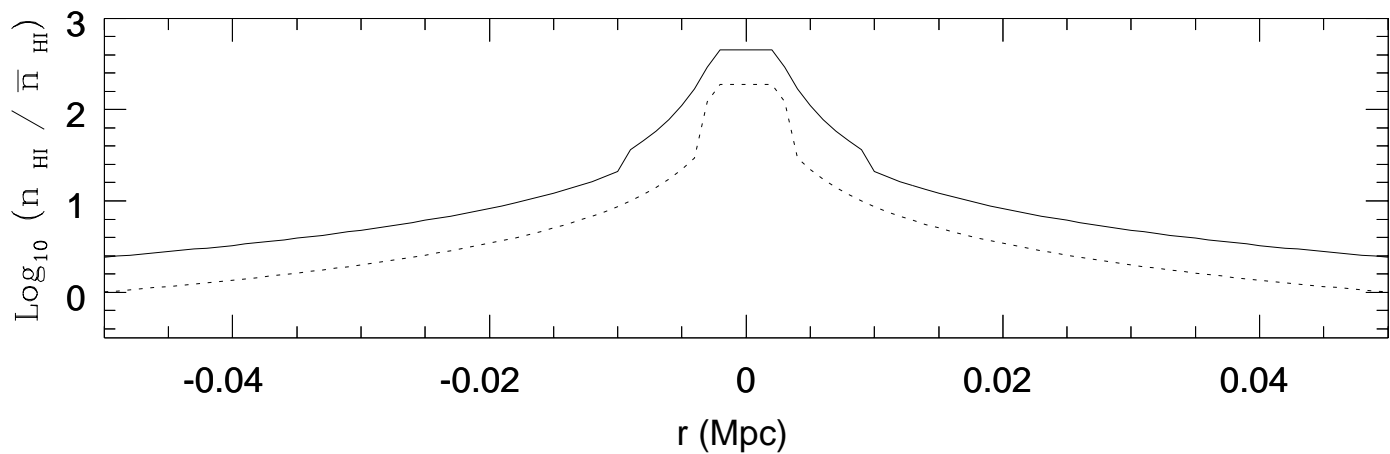
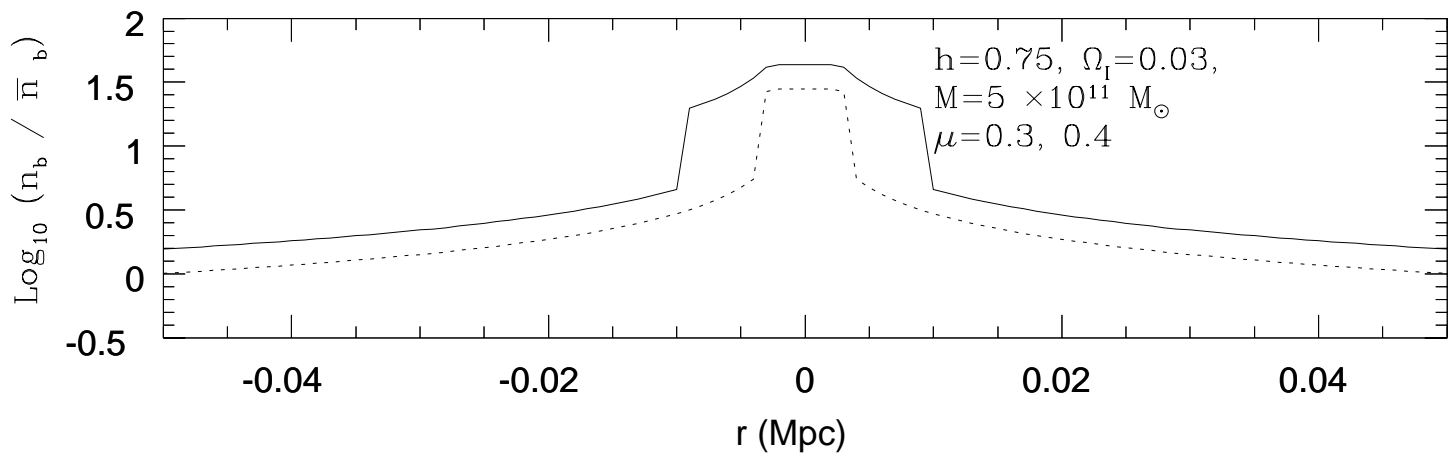


Fig. 2

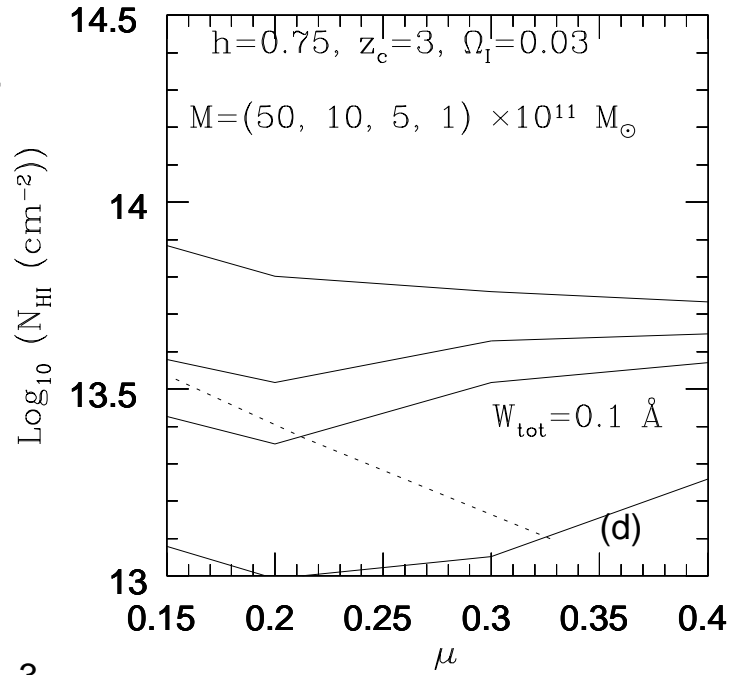
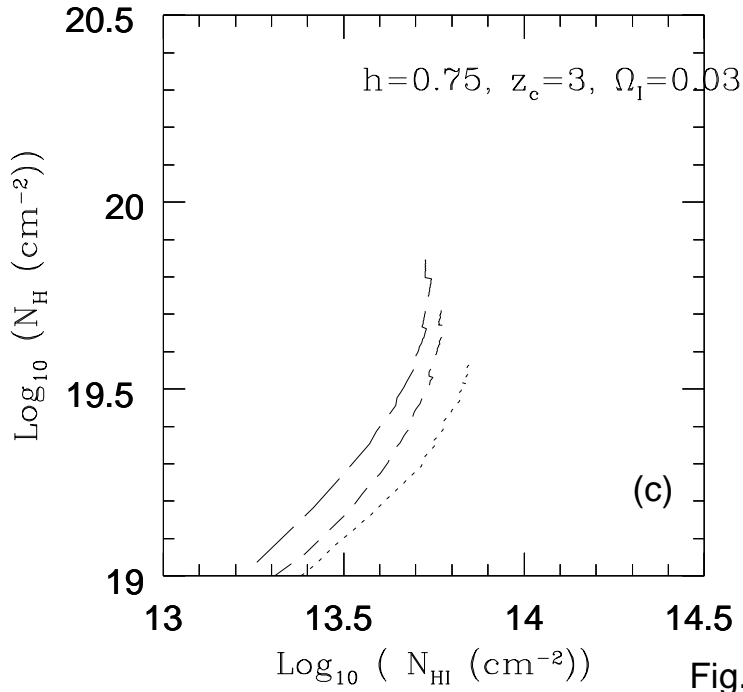
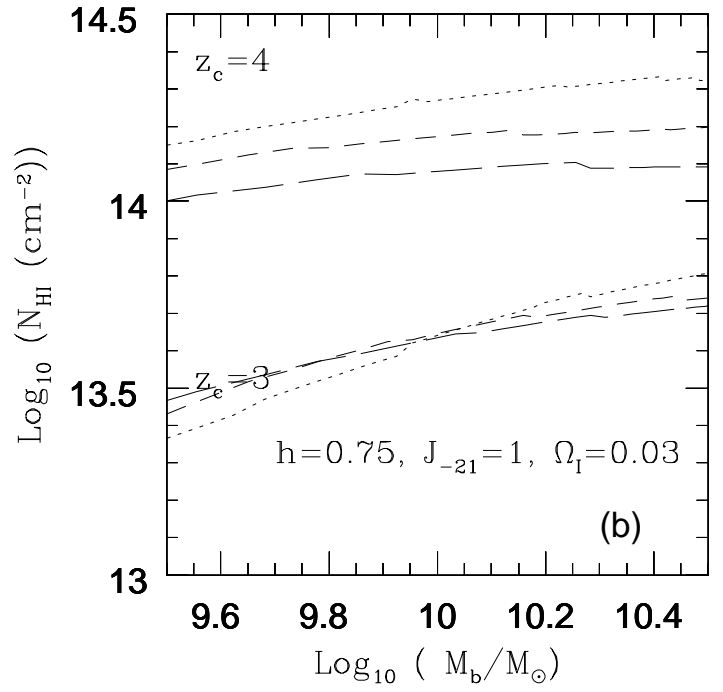
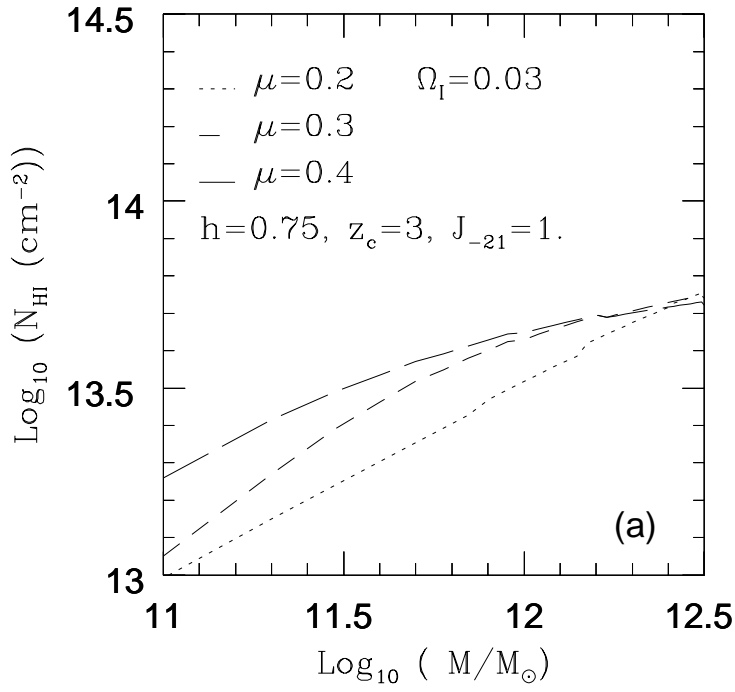


Fig. 3

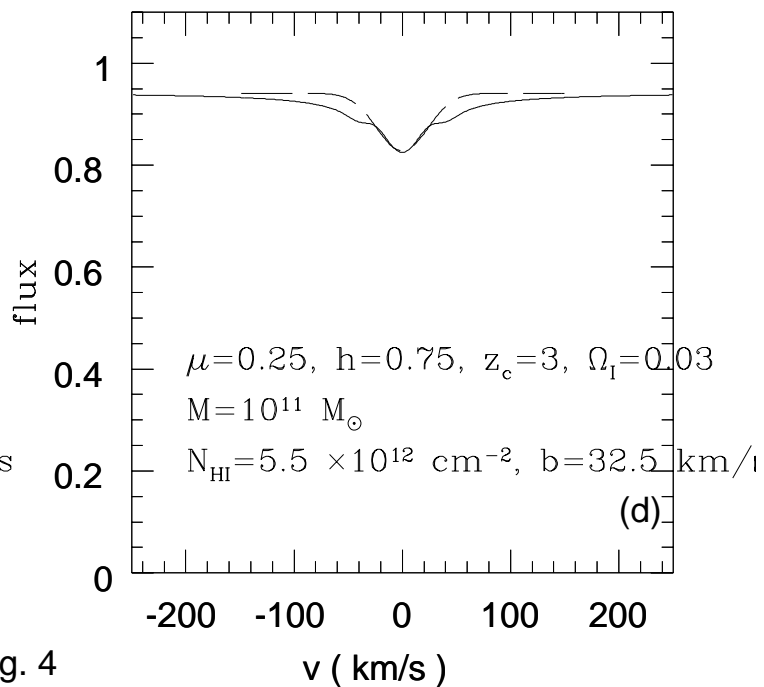
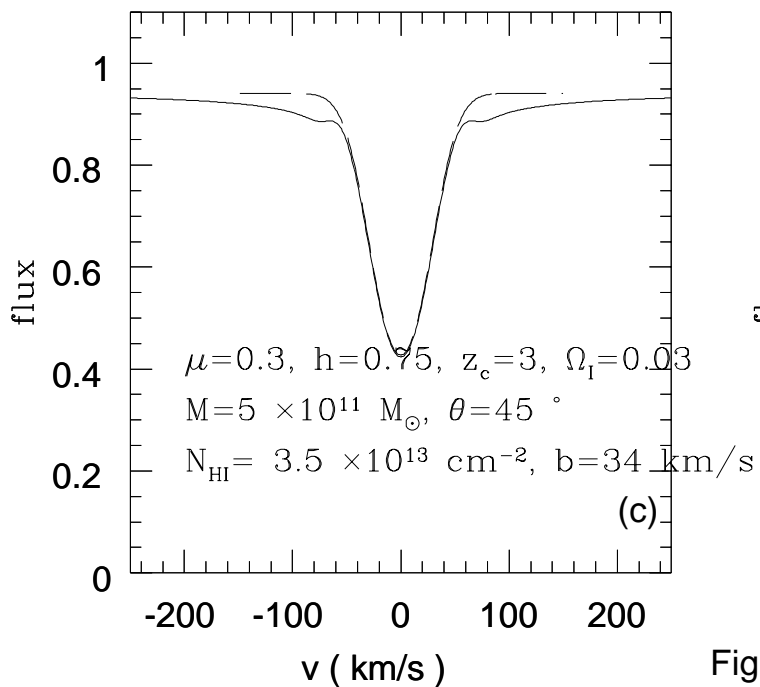
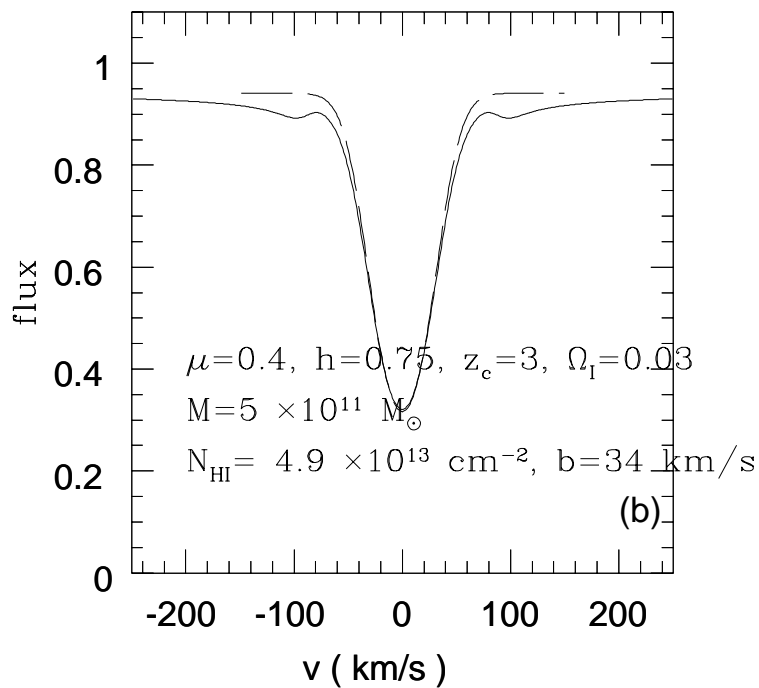
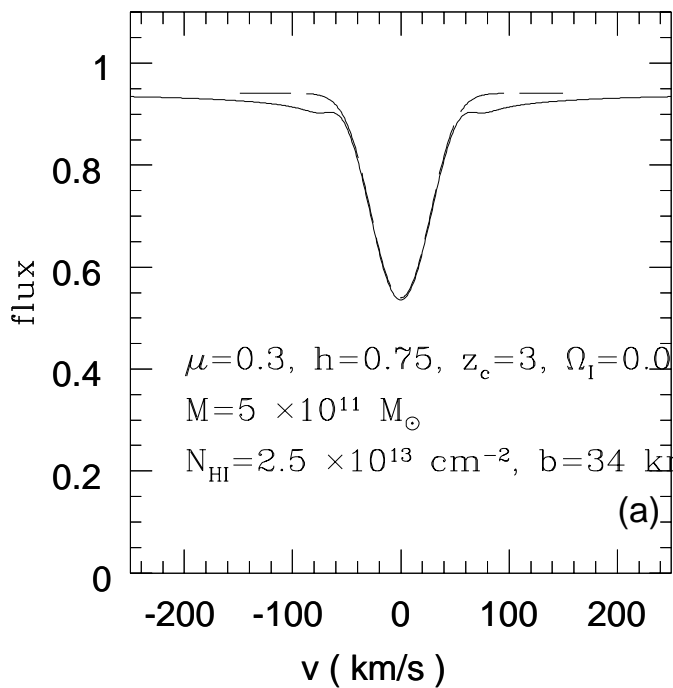


Fig. 4

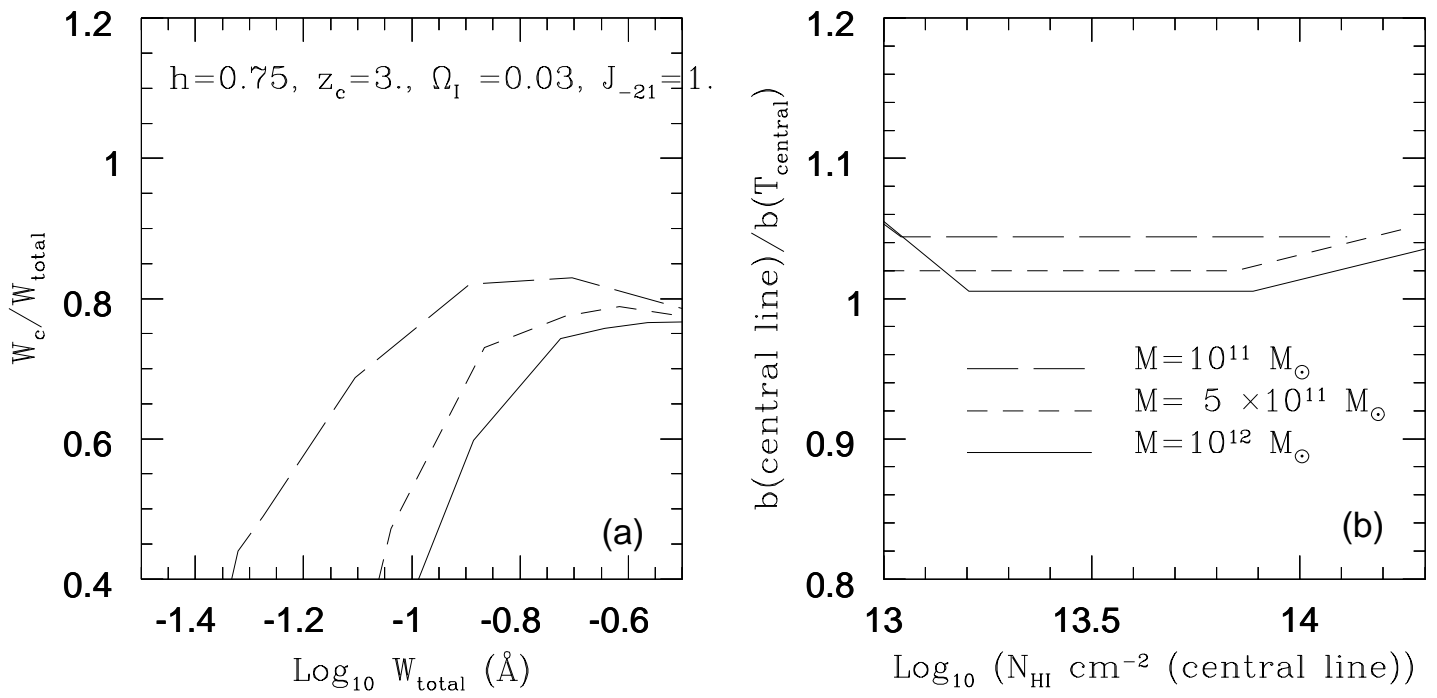


Fig. 5

